Available online at www.sciencedirect.com
SCIENCE DIRECT®
Journal of Catalysis 226 (2004) 16–24
JOURNAL OF CATALYSIS
www.elsevier.com/locate/jcat

Cobalt-exchanged hydroxyapatite catalysts: Magnetic studies, spectroscopic investigations, performance in 2-butanol and ethane oxidative dehydrogenations

Kaoutar Elkabouss [a,b], Mohamed Kacimi [a], Mahfoud Ziyad [a], Souad Ammar [b], François Bozon-Verduraz [b,*]

[a] *Laboratoire de Physico-Chimie des Matériaux et Catalyse, Faculté des Sciences, Département de Chimie, Rabat, Morocco*
[b] *Groupe de Chimie des Matériaux Divisés et Catalyse, ITODYS, UMR-CNRS 7086, Université Paris 7-Denis Diderot, case 7090, 2, place Jussieu, 75251 Paris cedex 05, France*

Received 27 January 2004; revised 3 May 2004; accepted 5 May 2004

Available online 5 June 2004

Abstract

A series of exchanged cobalt/calcium (Co^{2+}/Ca^{2+}) hydroxyapatite $Ca_{10-x}Co_x(PO_4)_6(OH)_2$ was synthesized and characterized by XRD, UV-visible-near-infrared (NIR) and IR spectroscopy, magnetic measurements (SQUID), and X-ray photoemission spectroscopy (XPS). The level of Co^{2+}/Ca^{2+} exchange was limited to 1.35 wt% Co. After calcination in air at 550 °C, cobalt was still present as Co^{2+} and all samples were paramagnetic, showing that the apatite matrix impedes the oxidation of Co^{2+} and that the Co^{2+} ions are isolated, whatever the Co content. Magnetic measurements and UV-visible diffuse reflectance spectra show that the exchanged Co^{2+} ions are hosted by two types of sites (with octahedral and trigonal prismatic symmetries). XPS confirmed the surface cobalt enrichment and did not reveal Co^{3+} ions. Dehydrogenation of 2-butanol leads almost exclusively to the formation of butanone. As the Co content increases, the ketone yield passes through a maximum. In the oxidative dehydrogenation of ethane, the ethylene yield also reaches a maximum (22 mol%) for 0.96 wt% Co at 550 °C. These results are ascribed to (i) the partial compensation of the intrinsic dehydrogenating activity of cobalt by the decrease in basicity of apatite induced by the replacement of Ca^{2+} by Co^{2+}, and (ii) the involvement of two types of sites.

Keywords: Cobalt catalysts; Hydroxyapatite; UV-visible-NIR diffuse reflectance; DC magnetic susceptibility; XPS; 2-Butanol dehydrogenation; Ethane oxidative dehydrogenation

1. Introduction

Phosphates with an apatite-like structure $M_{10}(PO_4)_6(OH)_2$, where M is a divalent cation, represent a large family of materials used in different applications such as: (i) ion exchangers for chromatographic columns or for the storage of heavy or radioactive elements, (ii) luminescent materials, (iii) bioceramics for implantation (rheumatoid arthritis), (iv) electrolytes for high-temperature fuel cells, and (v) catalysts [1–6].

Calcium hydroxyapatite $Ca_{10}(PO_4)_6(OH)_2$, CaHap, has a hexagonal unit cell, whose composition is highly flexible. The structure was described by Beevers and McIntyre [5] and confirmed by Young and co-workers [6]. It is a compact assemblage of $[PO_4]^{3-}$ and Ca^{2+}, which defines two types of zeolite-like channels. The first type of channel has a diameter of about 2.5 Å and contains Ca^{2+} ions, Ca^{2+}(I), surrounded by nine oxygen atoms. The second type of channel (3.5 Å in diameter) hosts the hydroxyl groups and pseudo-octahedral Ca^{2+}(II) cations, and plays an important role in the acid–base and electrical properties of apatite. The calcium ions can be exchanged with most divalent cations [7–10] without affecting the stability of the phosphate. With regard to the exchange abilities, there is no agreement between the researchers about the amount of exchangeable cations, but the order $Cu^{2+} > Pb^{2+} > Zn^{2+} > Cd^{2+} > Co^{2+}$ is generally accepted [8]. The kinetics of exchange is governed by the nature and the radius of the cation. Moreover,

* Corresponding author. Fax: 33 1 44 27 61 37.
E-mail address: bozonver@ccr.jussieu.fr (F. Bozon-Verduraz).

0021-9517/$ – see front matter
doi:10.1016/j.jcat.2004.05.007

the hydroxyl groups in the tunnels can be exchanged easily by Cl^-, F^-, and Br^- [3,10]. Other structural modifications are brought about by replacing phosphorus by vanadium or arsenic and by the creation of nonstoichiometry or calcium deficiency. All these changes influence the properties of the apatites and allow the modulation of their surface acid–base characteristics.

These features have attracted attention with regard to applications of phosphates and apatites in heterogeneous catalysis [4,11–24]. Hall and co-workers [11,12] demonstrated the efficiency of apatites in the dehydration and dehydrogenation of 2-butanol, and assigned the dehydrogenation activity to their basic character. Incorporation of transition-metal ions into alkaline earth phosphates improves their performance in dehydrogenation. Introduction of Cu^{2+} and Ni^{2+} ions into this matrix creates new redox centers [13] whereas the incorporation of Cu^{2+} induces activity in cyclohexane dehydrogenation [14]. On the mixed cobalt–calcium orthophosphates, $Ca_{3-x}Co_x(PO_4)_2$, the transformation of 2-propanol into acetone is favored, in contrast to $Ca_3(PO_4)_3$, and the dehydrogenation activity was ascribed to the formation of Co^{3+} ions during the thermal activation [15]. The oxidative dehydrogenation of light alkanes on CaHap and SrHap was studied in depth by Moffat and co-workers [16–19] and Sugiyama et al. [20]. CaHap catalyzes the partial oxidation of methane to carbon monoxide and hydrogen at about 600 °C [16]. The formation of oxygen radical species on both nonstoichiometric and stoichiometric calcium hydroxyapatites has been reported [17]. On CaHap, the selectivity to propene in the oxidative dehydrogenation of propane (ODHP) is increased significantly by adding tetrachloromethane [18]. In SrHaP, the introduction of cobalt by exchange [19] also enhances the selectivity to propene [20]. In the latter case, the activity of the Co-rich catalysts was ascribed to "active oxygen species derived from the abstraction of hydrogen from OH groups." Several investigators also proved that the addition of phosphorus improves the performances of various catalysts in the oxidative dehydrogenation of ethane (ODHE), although its role in the activity enhancement and in the structure of active sites is still unclear. For instance, El-Edrissi et al. [21] showed that the addition of phosphorus to Cr/TiO_2 and V_2O_5/TiO_2 increases the activity and the selectivity to ethylene. This was assigned to the appearance of new phosphate phases on the carrier and also to the tuning of the surface acid–base properties to the values necessary for the reaction.

The present work is a part of a study of the catalytic behavior of cobalt/CaHap systems in the oxidative dehydrogenation of ethane, carried out in our laboratories; it follows investigations of cobalt/titania [22] and cobalt/phosphate [23] systems. The use of cobalt is justified by its importance in redox catalysis. Concerning the cobalt sites, the question arises as to their *isolated* or *cooperative* nature. This prompted us to incorporate cobalt ions through ion exchange [19] and to carry out combined magnetic and spectroscopic (UV-visible-NIR) studies, in addition to XRD, IR, and XPS measurements. Moreover, the role of the acid–base properties of the solids was investigated by testing their performance in the dehydrogenation of 2-butanol in an attempt to correlate these properties with the catalytic performance (activity and selectivity) in ODHE.

2. Experimental

2.1. Preparation of the support and the catalysts

Several methods for the preparation of CaHap have been reported [10,24–26]. Most of these lead to pure Hap but do not produce the large surface area required for catalysis. This prompted us to use the following procedure: a solution of $(NH_4)_2HPO_4$ (0.6 mol L^{-1}) was added dropwise to a 1 mol L^{-1} solution of calcium nitrate while stirring. The resulting precipitate was slowly dissolved in 2 mol L^{-1} nitric acid. The solution was adjusted to pH 9, by adding ammonia, which led to a second precipitation; the pH was maintained while stirring at 80 °C for 24 h. After filtration, the recovered solid was washed well with hot water and dried at 80 °C and then at 120 °C.

The exchanged samples, Co/Hap, were prepared at room temperature by introducing 1 g of CaHap into 50 cm^3 of ultrapure water. After stirring for 24 h, a solution of cobalt nitrate of known concentration was added to the suspension, which was again stirred for 24 h. The solids recovered after filtration were washed with hot water, dried at 120 °C, and finally calcined at 550 °C in a rotating furnace flushed with air. The temperature of 550 °C is at least as high as the reaction temperature (450–550 °C) but not high enough to induce the formation of pyrophosphate [27]. The samples are labeled Co(z)Hap, where z is the Co wt% content; they are violet.

2.2. Characterization techniques

The specific surface area of the samples evacuated at 300 °C was measured using nitrogen adsorption at −196 °C. X-Ray diffraction patterns were obtained with a Siemens D500 high-resolution diffractometer using Co$K\alpha$ radiation ($\lambda = 1.78$ Å). The data were collected with a 0.02° (2θ) step at room temperature. Diffuse reflectance spectra were recorded at room temperature between 190 and 2500 nm on a Varian Cary 5E spectrometer equipped with a double monochromator and an integrating sphere coated with polytetrafluoroethylene (PTFE). PTFE was the reference. FTIR transmission spectra were recorded on a Bruker Equinox spectrometer between 4000 and 400 cm^{-1} using self-supporting and KBr disks. This technique was used because it provides information about the purity of the samples. It is sensitive to the presence of carbonates and pyrophosphates. Chemical analyses were carried out at the Service Central d'Analyse (CNRS, Vernaison) by inductive coupling plasma-atomic emission spectroscopy

(ICP-AES). DC magnetic susceptibility was measured on a SQUID magnetometer in the 5 to 300 K range with a magnetic field of 200 Oe. The data, corrected from the diamagnetic contribution of apatite, are presented per mole of cobalt.

X-ray photoelectron spectra were recorded on a SSX-100 spectrometer (Surface Science Laboratory) equipped with a monochromated Al$K\alpha$ source (1486.6 eV, 20 W) at about 10^{-9} Torr, and on a VG Scientific ESCALAB 250 system equipped with a micro-focused, monochromated Al$K\alpha$ X-ray source (1486.6 eV, 650 µm spot size, 200 W) and a magnetic immersion lens, which focuses electrons emitted from the sample over a cone of up to ±45° into the main lens column of the equipment. The magnetic immersion lens enhances the sensitivity by about one order of magnitude. The spectra were acquired in the constant analyzer energy mode, with a pass energy of 150 eV for the survey and 40 eV for the narrow regions. Furthermore, higher spectral resolution was achieved for the C1s and Si2p regions by setting the pass energy at 10 eV. The spectra were digitized, summed, smoothed, and reconstructed using Gauss-Lorentzian components. The measurements were carried out on powdered samples dispersed on an indium plaque, using the C1s peak at 285 eV as a reference. The surface composition of the samples was estimated from XPS peak areas corrected by the difference in cross sections according to Scofield data [28].

2.3. Catalytic tests

2-Butanol conversion was used as a probe reaction to evaluate the acid–base properties of the catalysts. The study was carried out between 120 and 240 °C in a U-shaped continuous-flow microreactor operating at atmospheric pressure. 2-Butanol diluted by air or N_2 was fed into the reactor at a partial pressure of $P_{ol} = 8.4 \times 10^2$ Pa; the total flow rate was 60 $cm^3\,min^{-1}$. The reaction mixture was analyzed by a FID chromatograph equipped with a stainless-steel column (diameter 1/8 inch) containing Carbowax 1500 (15%) on Chromosorb PAW (60/80 mesh). The selectivity to butanone is about 100% (99.5%) and the results are expressed in terms of butanone yield.

The oxidative dehydrogenation of ethane was performed from 400 to 550 °C in a quartz U-shaped fixed-bed microreactor operating at atmospheric pressure. Prior to the reaction, the catalyst was sieved to a grain size of 125 to 180 µm, then put into the reactor between two quartz wool plugs, and treated in a stream of pure nitrogen. The reaction mixture was 6 vol% ethane, 3 vol% O_2, and 91 vol% N_2 and the total flow rate was 60 $cm^3\,min^{-1}$. The effluent gases were analyzed by means of two on-line chromatographs: one equipped with a Porapak Q column and a FID, and the other equipped with a silica gel column and catharometers. Under the experimental conditions, the reaction started at around 300 °C and produced only ethylene and CO_x.

3. Results and discussion

3.1. Characterization of the samples

3.1.1. Chemical analysis

After calcination at 550 °C, the initial CaHap contains 37.38 wt% Ca and 17.39 wt% P, with a Ca/P ratio of 1.67. Hence, this hydroxyapatite is stoichiometric. The Co^{2+}/Ca^{2+} exchange characteristics were determined by adding the same amount of Hap to several solutions of different cobalt concentrations. Fig. 1 depicts the variation in the Co and Ca contents (wt%, measured after calcination at 550 °C) of the solid samples versus the initial Co content in the solutions (amount of Co introduced divided by the amount of Hap, before exchange). It shows clearly that the sum of the exchanged Co^{2+} ions and of the remaining Ca^{2+} ions is fairly constant and equal to the initial amount of Ca^{2+}. The exchange reaches a plateau at 1.35 wt% Co, i.e., a Co^{2+}/Ca^{2+} ratio of 0.023. In hydroxyapatite, the calcium cations occupy two sites: Ca^{2+}(I) surrounded by nine oxygens and Ca^{2+}(II) surrounded by seven oxygens. However, as shown in Table 1, the effective coordination is six for both sites because six oxygens are located between 2.41 to 2.45 Å from Ca^{2+}(I) and between 2.36 to 2.50 Å for Ca^{2+}(II), the other oxygens being 2.7 to 2.8 Å away [29]. It is noteworthy that the maximum exchanged Co (1.35 wt%) is lower than that obtained with copper, which is around 3.3 wt% [13]. However, the sizes of the cations are similar; the texture of the phosphate and the exchange media may thus play a role.

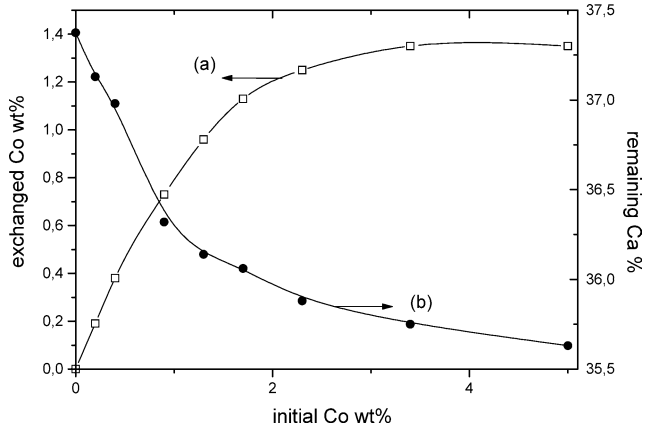

Fig. 1. Amounts of exchanged cobalt (a) and remaining calcium (b) versus initial Co content in the solution.

Table 1
Some structural information on calcium sites in CaHap

Site	Ca–O distances (Å)	Ca–P distances (Å)
Ca(I)	2.41(3), 2.45(3), 2.77(3)	3.0–3.7
Ca(II)	2.36(4), 2.5(2), 2.7(1)	

Table 2
Specific surface areas of the samples before and after ODHE reaction at 550 °C

Amount of cobalt (wt%)	0	0.19	0.38	0.73	0.96	1.13	1.25	1.35
Specific surface area ($m^2\ g^{-1}$) before catalysis	51	41	39	40	42	40	40	43
Specific surface areas ($m^2\ g^{-1}$) after ethane ODH	47	34	35	35	34	39	40	39

3.1.2. Surface area

The surface areas of CaHap and of the different Co(z)/Hap samples, before and after the catalytic tests, are reported in Table 2. The Co^{2+}/Ca^{2+} exchange lowers the Hap surface areas by approximately 20%.

3.1.3. XRD patterns

According to the XRD patterns, the exchanged samples calcined at 550 °C are isostructural with CaHap (JCPDS 9432). They were indexed in the hexagonal system with space group $P6_3/m$. The lattice parameters a and c were determined using the least-squares method. The incorporation of cobalt into $Ca_{10}(PO_4)_6(OH)_2$ resulted in a slight decrease in the parameter a, confirming that Co^{2+} ions are introduced into the phosphate network. The parameters of pure CaHap are $a = b = 9.424$ Å, $c = 6.877$ Å. For the Co(0.96)Hap sample, they are $a = b = 9.414$ Å, $c = 6.877$ Å, and for Co(1.35)Hap, $a = b = 9.399$ Å, $c = 6.876$ Å. This contraction of the unit cell is in agreement with the lower ionic radius of the Co^{2+} ion (0.735 Å) compared to Ca^{2+} (1.00 Å).

3.1.4. IR spectroscopy

The IR spectra of the samples are characteristic of CaHap. They exhibit three bands centered at 965, 1035, and 1094 cm^{-1}, attributed to the different vibrational modes of the P–O bond, and a sharp band at 3575 cm^{-1}, due to the symmetric vibrations (ν_s) of the OH groups in the channels of the structure [9]. Cobalt exchange does not modify the vibrational modes of the different bonds in CaHap. The samples do not contain pyrophosphate, since the bands due to the stretching modes of $P_2O_7^{4-}$ (1165, 1124, and 757 cm^{-1}) are absent from the spectra [30].

3.1.5. UV-visible-NIR DRS

The UV-visible-NIR spectra of Co(z)Hap samples are displayed in Fig. 2 on the Schuster-Kubelka-Munk (SKM) scale. The spectrum of CaHap (not shown) consists mainly of a band at 296 nm, attributed to $O^{2-} \rightarrow Ca^{2+}$ charge transfer, and of several bands in the near infrared (NIR) due to: (i) $\nu_{(OH)}$ overtones of surface hydroxyl groups (1386 and 1432 nm) and (ii) a combination of $\nu_{(OH)}$ and $\delta_{(OH)}$ (1940 and 2220 nm). After exchange of different quantities of cobalt, the spectra show a weak band at 325 nm, a set of three bands at 520, 570, and 640 nm, and a broad band from 1100 to 1800 nm, partially overlapping with OH overtones. The weak band at 325 nm is ascribed to a spin-forbidden transition and will not be considered further.

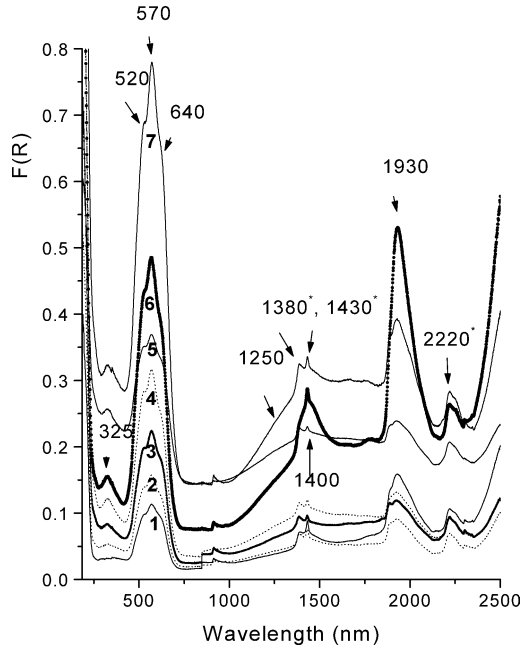

Fig. 2. UV-visible-NIR diffuse reflectance spectra of Co(z)/Hap for different z (wt%) values: (1) 0.19; (2) 0.38; (3) 0.73; (4) 0.96; (5) 1.13; (6) 1.25; (7) 1.35.

In most oxygen environments, cobalt is present as high-spin $Co^{2+}(3d^7)$ and/or low-spin $Co^{3+}(3d^6)$. In the high-spin configuration, free Co^{2+} ions display a ^4F fundamental term and a ^4P excited term. In octahedral symmetry, three spin-allowed d–d transitions appear: $\nu_1[(^4T_{1g}(F) \rightarrow {}^4T_{2g}(F)]$, $\nu_2[(^4T_{1g}(F) \rightarrow {}^4A_{2g}(F)]$, and $\nu_3[(^4T_{1g}(F) \rightarrow {}^4T_{1g}(P)]$; since the $^4A_{2g}(F)$ and $^4T_{1g}(P)$ levels cross, the ν_2 and ν_3 transitions are poorly resolved, their separation depending on the cobalt–oxygen distance. In tetrahedral symmetry, the three spin-allowed d–d transitions, $\nu_1[^4A_2(F) \rightarrow {}^4T_2(F)]$, $\nu_2[(^4A_2(F) \rightarrow {}^4T_1(F)]$, and $\nu_3[(^4A_2(F) \rightarrow {}^4T_1(P)]$ are also symmetry allowed [31]. As the levels do not cross, these transitions are well separated but ν_1, which lies in the IR range, is rarely observed. *In both these high symmetry surroundings*, the T levels are generally split, for several reasons: (i) lowering of symmetry arising from distortions, (ii) spin–orbit coupling, and (iii) the dynamic Jahn-Teller effect. Moreover, five coordination is not uncommon in cobalt complexes [32,33]. Hence, identification of Co^{2+} sites is not straightforward. However, significant information is given by the band intensity, much higher in a tetrahedral environment (due to symmetry allowance) and by comparison with model compounds. The following model compounds are rel-

Table 3
Position and attribution of UV-visible-NIR bands of Co/Hap samples

Band position (nm)	Band position (cm^{-1})	Attribution d–d transition
516	19400	$^4T_{1g}(F) \rightarrow {}^4T_{1g}(P)$ O_h
		$4A'^2(F) \rightarrow {}^4E''(P)$ D_{3h}
570, 644	17500, 15500	$\nu_2({}^4T_{1g}(F) \rightarrow {}^4A_{2g}(F))$ O_h
		$4A'^2(F) \rightarrow {}^4A'^2(P)$ D_{3h}
1250	8000	$\nu_1({}^4T_{1g}(F) \rightarrow {}^4T_{2g}(F))$ O_h
1400–1800	7150–5550	$4A'^2(F) \rightarrow {}^4E'$ D_{3h}

evant: (i) O_h symmetry encountered in Co^{2+}/MgO [34,35] and β-$Co(OH)_2$ [36], (ii) six-coordinated trigonal prism D_{3h}, (iii) five-coordinated C_{3v} or D_{3h} in Co^{2+}/zeolite [37–39], (iv) five-coordinated C_{4v} observed in $(MgCo)_2P_2O_7$ [40], (v) T_d symmetry in Co^{2+}/ZnO [41]. The latter two sites can be ruled out: $(MgCo)_2P_2O_7$, which displays a band around 835 nm, not observed in this study, and the tetrahedral species because the band intensity is too low [22, 31,39]. Conversely, the presence of an octahedral oxygen environment is supported by comparison with the spectral features of Co^{2+}/MgO [31,34] and β-$Co(OH)_2$ [36], except for the absorption in the 1400 to 1800 nm range (Table 3); this suggests that another Co^{2+} site is involved. This second species may be identified with C_{3v}-sited Co^{2+} and six- or five-coordinated D_{3h} species. The attributions proposed are presented in Table 3: (i) the shoulder at 516 nm is ascribed to $\nu_3[{}^4T_{1g}(F) \rightarrow {}^4T_{1g}(P)]$ whereas the peak at 570 nm and the shoulder at 644 nm are assigned to $\nu_2[{}^4T_{1g}(F) \rightarrow {}^4A_{2g}(F)]$; the splitting of this transition is due to spin–orbit coupling and/or Jahn-Teller perturbation [31,39]; C_{3v} or D_{3h} entities also absorb in this region, (ii) in the 1100–1800 nm region, the shoulder near 1250 nm is ascribed to the ν_1 transition $[{}^4T_{1g}(F) \rightarrow {}^4T_{2g}(F)]$ of an octahedral species, whereas absorption in the 1400–1800 nm range is assigned to the ν_1' transition $[4A'^2(F) \rightarrow {}^4E'(F)]$ of the D_{3h} environment (probably six-coordinated). It is noteworthy that Co^{2+} ions are exchanged with surface Ca^{2+} ions (see XPS data below). For these surface Co^{2+} ions, the missing oxygens are replaced by water molecules, which leads to six-coordinated cations with more or less marked distortions from the octahedral. It is important to note that the Co^{3+} ions are absent, despite the treatment at 550 °C in air, proving a marked support effect, i.e., the apatite matrix impedes the oxidation of Co^{2+} in air.

3.1.6. Magnetic measurements

For a free high-spin Co^{2+} ion ($^4F_{9/2}$ fundamental state), the calculated effective magnetic moment μ_{eff}, involving a full orbital contribution, is about 6.63 μ_B [42]; in octahedral six-coordinate oxygen complexes where the fundamental electronic state is ^4T, the typical experimental μ_{eff} value of Co^{2+} ion ranges from 4.70 to 5.20 μ_B [43]. A μ_{eff} value of 6.63 μ_B, which approaches the expected full orbital contribution, has been reported for octahedrally coordinated Co^{2+} ions in aluminosilicate glasses containing 40 mol% CoO [44]. Conversely, when the fundamental state is orbitally nondegenerate ($^4A_2$) or partially degenerate (^4E), the orbital contribution is fully or partially quenched and the experimental μ_{eff} values lie in the 3.9 to 4.4 range, close to the spin-only value (about 3.88 μ_B) [45].

The temperature dependence of the reciprocal magnetic susceptibility (χ_M^{-1}) of all the tested catalysts is presented in Fig. 3 and is compared to that of the antiferromagnetic standard Co_3O_4. The Curie law is verified for all the samples, suggesting that the cobalt ions are magnetically isolated. The effective magnetic moment μ_{eff} is deduced from the slope of the χ_M^{-1} vs T plot (obtained by a least-square linear fit) in the whole temperature range. For 0.19 wt% Co, the value is high (5.98 μ_B), but for Co-richer samples, μ_{eff} is close to 4.1–4.3 μ_B, with the exception of the sample containing 0.96 wt% Co, which amounts to 4.91 μ_B (Table 4). These μ_{eff} values confirm that the cobalt ions are predominantly in the bivalent state and suggest that their siting changes with the cobalt composition.

If we ignore the highest μ_{eff} values, obtained for $z = 0.19$ and 0.96 wt%, the average μ_{eff} value is close to the spin-only value (about 3.88 μ_B) [45]; this suggests almost complete quenching of the orbital contribution. This occurs in four-coordinated tetrahedral (Td), five-coordinated (C_{4v}, C_{3v}, C_{2v} or D_{3h}), or six-coordinated (D_{3h} trigonal prism) high-spin complexes [27,34].

Another possible explanation for the lower μ_{eff} values is the partial antiferromagnetic spin coupling through bridging oxygen ligands. This hypothesis can be evaluated through examination of the $\chi T(T)$ curves (Fig. 4). For the samples at 0.73, 1.13, and 1.35 wt% Co, the χT value is almost

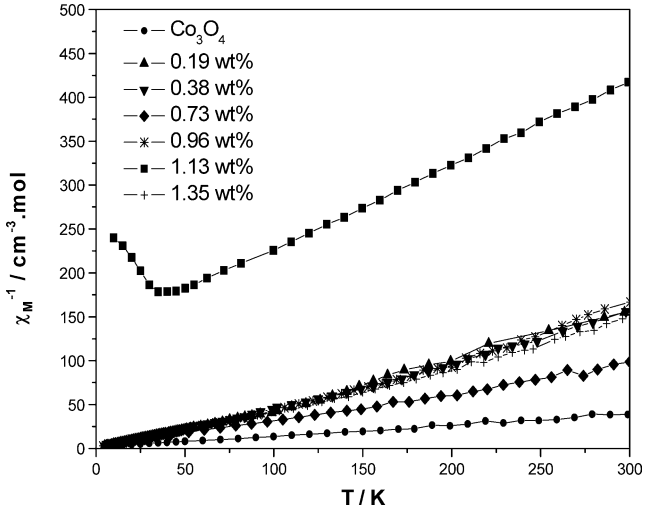

Fig. 3. Temperature dependence of the reciprocal susceptibility of catalysts (the curve of Co_3O_4 is also shown for comparison).

Table 4
Effective magnetic moment of cobalt ions in Co/Hap samples

Co (wt%)	0.19	0.38	0.73	0.96	1.13	1.35
μ_{eff} (μ_B)	5.98	4.28	4.28	4.91	4.22	4.14

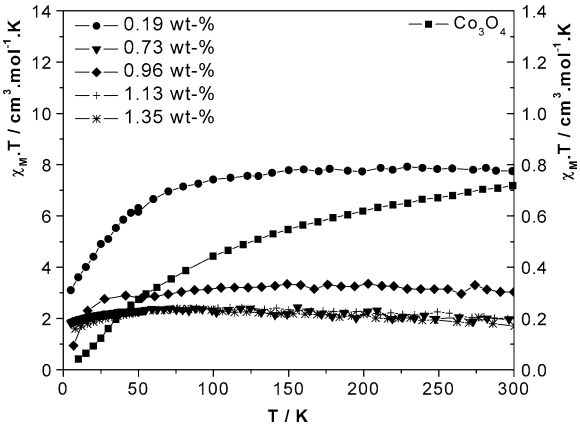

Fig. 4. Temperature dependence of χT for catalysts with 0.19 to 1.35 Co wt% (for comparison, the curve of standard Co_3O_4 is also given).

constant from 300 to 5 K, which rules out antiferromagnetic coupling. However, for the two samples at 0.19 and 0.96% Co, χT is constant down to about 50 K but decreases at lower temperatures. This indicates the absence of antiferromagnetic coupling and the *occurrence of spin–orbit coupling in these samples*, high for the former, and less marked for the latter. Conversely, for Co_3O_4, where antiferromagnetic coupling occurs between Co^{2+} ions, χT decreases continuously with decreasing temperature. Hence, the higher μ_{eff} value of the samples at 0.19% Co (and to a lesser extent at 0.96% Co) is indicative of Co^{2+} siting (in majority) in a highly symmetric field such as an octahedral oxygen environment, in which the orbital contribution is important.

3.1.7. X-ray photoelectron spectra (XPS)

In practice, the identification of cobalt oxidation states is not straightforward because in many oxide systems, the Co2p binding energy (BE) of Co^{2+} exceeds that of Co^{3+} and the Co^{2+} reference compounds are often suspected to contain surface Co^{3+} [46]. However, the following are relevant: (i) the Co2p BE of Co^{2+} is slightly higher than that of Co^{3+} (781–783 and 779–780 eV, respectively); (ii) the Co2p spectrum shows a strong satellite (shake up) structure in high-spin Co^{2+} which is not observed in low-spin Co^{3+}; (iii) the spin–orbit splitting is higher in Co^{2+} species (about 15.7–16.0 eV) than in Co^{3+} species (15.0–15.5 eV) [22,38,46].

Table 5 gives the $Co2p_{3/2}$ BE, the surface $(Co/Ca)_{XPS}$ ratio (determined from the integrated areas of Co2p and Ca2p peaks) compared to the bulk values (determined by ICPMS), the spin–orbit coupling ΔE ($Co2p_{1/2} - Co2p_{3/2}$), and the S/M (satellite peak/main peak) intensity ratio. It appears that the $(Co/Ca)_{XPS}$ ratio is about four to five times the global ratio, which confirms that the exchange involves surface sites only. The values of BE and ΔE are characteristic of Co^{2+} ions and do not vary significantly as the amount of exchanged cobalt increases. Moreover, the S/M intensity ratio is nearly constant ($\geqslant 0.7$). It follows that cobalt ions are present exclusively as Co^{2+} species, in agreement with the data of UV-visible-PIR spectroscopy. On the other hand, examination of O1s BE may give some insight into the basicity of the samples. BE increases from about 529 eV for the most basic oxides to around 533 eV for the most acidic oxides [47]. The values of the Co(z)/HaP samples range from 531.2 for CaHap to 531.7 eV for $z = 1.35\%$, suggesting that the introduction of cobalt induces a slight decrease in basicity.

3.2. Catalytic activity

3.2.1. 2-Butanol conversion

The influence of the acid–base character of catalysts on the alkene selectivity in the ODH of alkanes is now recognized as an important parameter [48] and 2-butanol conversion is considered to be an important criterion [11,12]. In the present work, the stationary state activity of Co(z)Hap in 2-butanol conversion was investigated at different temperatures as a function of the quantity of exchanged cobalt (Fig. 5). In the absence of oxygen, the catalysts are not active below 220 °C and, moreover, the conversion does not exceed 1.4% above 220 °C. Hence, all experiments were performed in the presence of oxygen, whereupon a noticeable activity appears at $T \geqslant 160$ °C. The reaction produces almost exclusively butanone, with a negligible residual dehydration reaction (less than 0.5%). *On pure CaHap*, the butanone yield increases markedly with temperature and amounts to 86% at 240 °C (Fig. 5); this dehydrogenation activity can be ascribed to basic centers such as Ca^{2+}–O^{2-} pairs, which can abstract hydrogen atoms. *On Co(z)Hap samples*, the butanone yield increases with temperature in the 160 to 240 °C range and clearly reaches a maximum at around $z = 0.3$–0.5, shifting toward higher values of z upon temperature increase (Fig. 5).

This maximum may be related to: (i) the involvement of different Co^{2+} sites, as shown by UV-visible spectra and

Table 5
XPS data

Sample z (wt%)	$Co2p_{3/2}$ BE/eV	Ca at.%	Co at.%	Co/Ca XPS at.%	Co/Ca bulk at.%	ΔE	S/M
0.19	782.3	21.24	0.27	1.27	0.32	15.7	0.78
0.38	783.0	15.68	0.85	3.36	0.64	15.7	0.72
0.73	783.0	21.35	1.22	5.71	1.20	15.4	0.76
0.96	782.5	19.59	1.02	5.21	1.60	15.7	0.76
1.35	782.7	19.55	2.54	12.99	2.30	15.6	0.69
Co_3O_4	780.0	–	–	–	–	15.1	

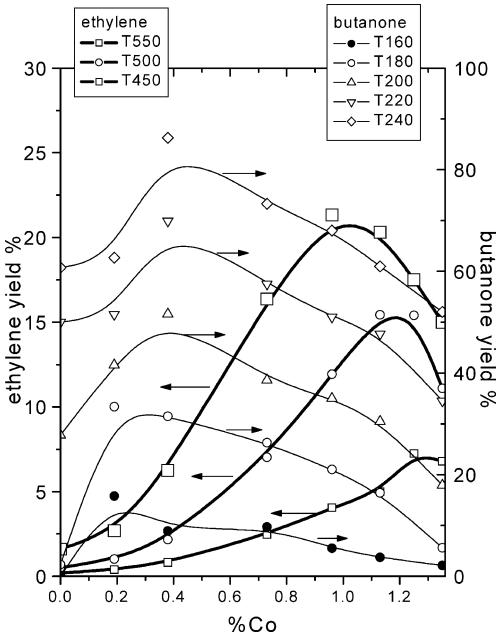

Fig. 5. Variation of butanone and ethylene yields with cobalt content.

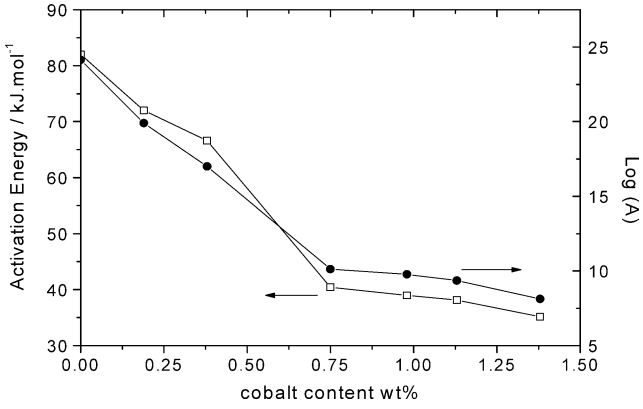

Fig. 6. 2-Butanol dehydrogenation: variation of activation energy and pre-exponential factor with cobalt content.

magnetic measurements, and (ii) the modification of the acid–base properties of the catalyst, induced by the incorporation of Co^{2+} ions. It is expected that this substitution will decrease the basicity of the solid by lowering the residual charge on the oxygen bonded to calcium. A maximum may be reached as a result of compensation between the specific dehydrogenating activity of Co^{2+} ions and the decrease in basicity. This duality also appears in the change in the apparent activation energy E_a and in the preexponential factor A with the amount of exchanged cobalt (Fig. 6). Both curves exhibit two domains: when the Co concentration increases; E_a and A decrease first but do not vary significantly for higher contents (> 0.75 wt%). However, this value is larger than that corresponding to the maximum butanone yield. This is due to the simultaneous occurrence of two mechanisms or two types of sites.

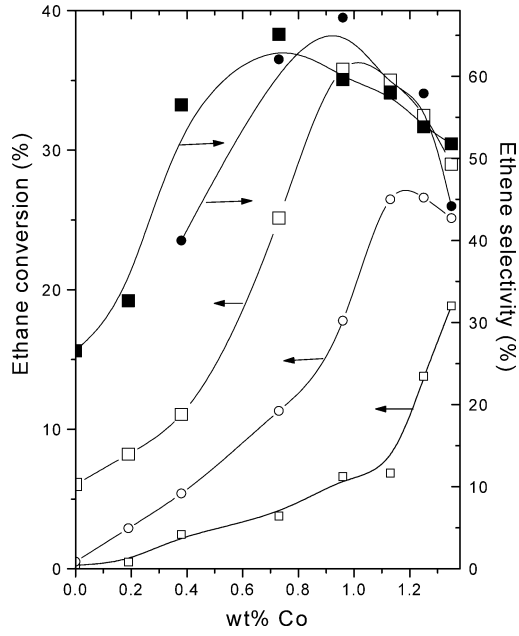

Fig. 7. Variation of ethane conversion (open symbols) and ethylene selectivity (full symbols) with cobalt content at different temperatures. The selectivity data at 450 °C, very close to those recorded at 500 °C, have been omitted for clarity. Symbols: small squares: 450 °C; circles: 500 °C; large squares: 550 °C.

3.2.2. Ethane ODH

The catalytic activity of Co(z)Hap samples was measured in the 400 to 550 °C range. Fig. 7 shows the variations in ethane conversion and ethylene selectivity with cobalt content. At 450, 500, and 550 °C, the conversion increases with the amount of cobalt but reaches a maximum at about 1 wt% Co at 550 °C. At 500 and 550 °C ethylene selectivity shows similar variations but a maximum is reached between 0.8 and 1%. As pointed out above for 2-butanol dehydrogenation, these maximums are due to the competition between the decrease in the basicity of oxygen upon cobalt incorporation into the apatite matrix, and the increase in dehydrogenating activity ascribed to Co^{2+}. Fig. 5 shows clearly that, to reach the maximum, a larger amount of cobalt is necessary than that for butanone production. The specific dehydrogenating performance of Co^{2+} (high selectivity) may be related to:

(i) the nature of the cobalt–hydrocarbon interaction, which could involve a hydride-like (Co^{2+}- -H–C_2H_5) species and an intermediate cobalt–ethylene species;

(ii) the nature of the active oxygen species involved. O_2^-, O^-, and O^{2-} (lattice) entities have been proposed for light alkanes dehydrogenation mechanisms, especially on vanadium-based catalysts; however, it is generally accepted that O_2^- is associated with nonselective oxidation [49]. O_2^- species have been detected at room temperature on pure CaHap outgassed at 900 °C [17]. On the other hand, the interaction of gaseous oxygen with Co^{2+} ions diluted in oxide matrices, such as MgO [50], has been shown to generate O_2^-

species at room temperature according to the equation:

$$Co^{2+} + \frac{1}{2}O_2 \rightleftarrows Co^{3+} + O_2{}^{-}.$$

However, under our reactions conditions ($T \geqslant 450\,^{\circ}C$), it is unlikely that $O_2{}^{-}$ contributes to selective oxidation.

The redox properties of $Ca_{3-x}Co_x(PO_4)_2$ in 2-propanol dehydrogenation were ascribed to the Co^{3+}/Co^{2+} couple [19]. Conversely, in Co(z)/CaHap (present work), the stabilization of Co^{2+} ions was shown by UV-visible spectroscopy, magnetic measurements, and XPS. We propose that the incorporation of Co^{2+} ions into the matrix favors the mobility of neighboring lattice oxygen or OH groups. As suggested by Sugiyama et al. [20] for propane oxidation on Co-SrHaP, active lattice oxygens may arise from the OH groups of the matrix. Moreover, above 500 °C, the OH groups are mobile enough to contribute to ionic conduction by diffusion, along the c axis of the hexagonal matrix of CaHap [51,52]. Hence, incorporation of cobalt should favor the formation of vacancies, which may be replenished by gaseous oxygen and contribute to ethylene production,

$$C_2H_6 + O_o \rightarrow C_2H_4 + H_2O + V_o,$$
$$\frac{1}{2}O_2 + V_o \rightarrow O_o,$$

where O_o is a lattice oxygen ion and V_o a neutral oxygen vacancy (containing two electrons).

Finally, at 550 °C, the maximum corresponds to an overall conversion approaching 35% and an ethylene yield of 22%, which is comparable with the best results achieved thus far over different catalysts in conventional reactors [48].

3.3. Characterization after ethane ODH

The surface area of the samples decreases slightly (Table 1), but analysis by XRD, UV-visible spectroscopy, and XPS did not show modification of other characteristics. Analogous stability was previously observed at similar reaction temperatures in hydrotreatment reactions over cobalt and molybdenum-loaded CaHap [53].

4. Conclusion

Introduction of cobalt by exchange in stoichiometric calcium hydroxyapatite, CaHap, is limited to 1.35 wt% Co. Even after calcination at 550 °C in air, cobalt is still present as Co^{2+}, which illustrates the effect of the support. According to UV-visible-NIR spectroscopy and magnetic measurements, cobalt is present as *isolated* Co^{2+} species, showing paramagnetism whatever the Co content. Two types of sites are involved: octahedral and probably six-coordinated D_{3h} (trigonal prism). Co(z)Hap samples are active in 2-butanol dehydrogenation in the presence of oxygen at $T \geqslant 160\,^{\circ}C$ with a selectivity in butanone of about 100%. The maximum butanone yield passes through a maximum for $z = 0.3$–0.5 wt% Co. It may involve different Co^{2+} sites and compensation between the decrease in apatite basicity and the increase in lattice oxygen mobility, induced by cobalt incorporation. Co(z)Hap catalysts show significant activity in ethane ODH at $T \geqslant 450\,^{\circ}C$, which increases with temperature in the 450 to 550 °C range. Upon increasing Co content, the ethylene yield reaches a maximum for $z \approx 1\%$ Co at 500 and 550 °C (22%), which can also be accounted for by the parameters discussed for 2-butanol conversion. Further work in progress on the ODH of propane shows that the propene yield is slightly lower (17%) than the ethylene yield, although propane is thermodynamically less stable than ethane.

Acknowledgments

The authors are indebted to the French Ministère des Affaires Etrangères for financial support (Action intégrée 183/MA/99). The XPS group of the ITODYS Laboratory (Université Paris 7-Denis Diderot) is gratefully acknowledged. We appreciate the help of C. Potvin (Laboratoire de Réactivité de Surface, Université Pierre et Marie Curie, Paris) for the XRD measurements and of P. Monod (ESPCI, Paris) for the magnetic measurements.

References

[1] J.C. Elliott, Structure and Chemistry of the Apatites and Other Calcium Orthophosphates, Elsevier, Amsterdam, 1994.
[2] J.C. Elliott, E. Bres, P. Hardouin (Eds.), Calcium Phosphate Materials, Sauramps Medical, Montpellier, 1998, p. 25.
[3] A. Lebugle, C. Rey, in: Biomémitisme et Matériaux, vol. 25, Observatoire Français des Techniques Avancées, Arago, 2000, p. 93;
J.W. Brodack, E. Deutsch, K. Deutsch, International patent WO 97/01304.
[4] J.B. Moffat, Catal. Rev.-Sci. Eng. 18 (1978) 199.
[5] C.A. Beevers, D.B. McIntyre, Miner. Mag. 27 (1944–1946) 254.
[6] M.I. Kay, R.A. Young, A.S. Posner, Nature 204 (1964) 1050.
[7] T. Suzuki, T. Hatsushika, Y. Hayakawa, J. Chem. Soc., Faraday Trans. 1 77 (1981) 1059;
T. Suzuki, K. Ishigaki, M. Miyake, J. Chem. Soc., Faraday Trans. 1 78 (1982) 3605;
T. Suzuki, K. Ishigaki, M. Miyake, J. Chem. Soc., Faraday Trans. 1 80 (1984) 3157.
[8] M. Wakamura, K. Kandori, T. Ishikawa, Colloids Surf. 164 (2000) 297;
S. Sugiyama, H. Matsumoto, H. Hayashi, J.B. Moffat, Colloids Surf. 169 (2000) 17.
[9] K. Yamashita, H. Owada, T. Kanazawa, T. Umekaki, Solid State Ionics 28–30 (1988) 660.
[10] T. Ishikawa, Stud. Surf. Sci. Catal. 99 (1996) 301.
[11] J.A.S. Bett, W.K. Hall, J. Catal. 10 (1968) 105.
[12] C.L. Kibby, W.K. Hall, J. Catal. 29 (1973) 144.
[13] M. Misono, W.K. Hall, J. Phys. Chem. 77 (1973) 791.
[14] A. Benarafa, M. Kacimi, G. Coudurier, M. Ziyad, Appl. Catal. 196 (2000) 25.
[15] A. Legrouri, J. Lenzi, M. Lenzi, React. Kinet. Catal. Lett. 48 (1992) 349;

A. Legrouri, S. Rhomdane, J. Lenzi, M. Lenzi, G. Bonel, J. Mater. Sci. 31 (1996) 2469.
[16] Y. Matsumura, J.B. Moffat, J. Catal. 148 (1994) 323.
[17] Y. Matsumura, H. Kanaï, J.B. Moffat, J. Mol. Catal. A 115 (1997) L229;
Y. Matsumura, H. Kanaï, J.B. Moffat, J. Mol. Catal. A 135 (1998) 317.
[18] S. Sugiyama, E. Nitta, H. Hayashi, J.B. Moffat, Catal. Lett. 59 (1999) 67;
S. Sugiyama, E. Nitta, H. Hayashi, J.B. Moffat, Appl. Catal. A 198 (2000) 171.
[19] S. Sugiyama, T. Moriga, M. Goda, H. Hayashi, J.B. Moffat, J. Chem. Soc., Faraday Trans. 92 (1996) 4305.
[20] S. Sugiyama, T. Shono, D. Makino, T. Moriga, H. Hayashi, J. Catal. 214 (2003) 8;
S. Sugiyama, H. Hayashi, Int. J. Mod. Phys. B 17 (2003) 1476.
[21] J. El-Edrissi, M. Kacimi, M. Loukah, M. Ziyad, J. Chim. Phys.-Chim. Biol. 94 (1997) 1984;
J. El-Edrissi, M. Kacimi, M. Loukah, F. Bozon-Verduraz, M. Ziyad, Catal. Lett. 56 (1998) 221.
[22] Y. Brik, M. Kacimi, M. Ziyad, F. Bozon-Verduraz, J. Catal. 202 (2001) 118;
Y. Brik, M. Kacimi, M. Ziyad, F. Bozon-Verduraz, J. Catal. 211 (2002) 470.
[23] A. Aadane, M. Kacimi, M. Ziyad, Catal. Lett. 73 (2001) 47.
[24] M. Jarcho, C.H. Bolen, M.B. Thomas, J. Bobick, J.F. Kay, R.H. Doremus, J. Mater. Sci. 11 (1976) 2027.
[25] D.M. Liu, T. Troczynski, W.J. Tseng, Biomaterials 22 (2001) 1721.
[26] M.A. Fanovich, J.M. Porto Lopez, J. Mater. Sci. Mater. Med. 9 (1998) 53;
A. Jillavenkatesa, S.R. Condrate, J. Mater. Sci. 33 (1998) 4111.
[27] S. Sugiyama, J.B. Moffat, Catal. Lett. 76 (2001) 75.
[28] J.H. Scofield, J. Electron Spectrosc. Relat. Phenom. 8 (1976) 129.
[29] A.S. Posner, A.F. Diorio, Acta Crystallogr. 11 (1958) 308.
[30] H. Tanaka, M. Chikazawa, K. Kandori, T. Ishikawa, Phys. Chem. Chem. Phys. 2 (2000) 2647;
M. Andrés-Vergés, C.M. Fernàndez-Gonzàlez, C. Martinez-Gallego, J.D. Solier, I. Cachadinà, E. Matijevic, J. Mater. Res. 15 (2000) 2526.
[31] B.P. Lever, Inorganic Electronic Spectroscopy, second ed., Elsevier, Amsterdam, 1984, p. 480.
[32] M. Ciampolini, I. Bertini, J. Chem. Soc. A 9 (1968) 2241.
[33] J.S. Wood, Inorg. Chem. 7 (1968) 852.
[34] M.L. Jacono, M. Cimino, Gazz. Chim. Ital. 103 (1973) 1281.
[35] A. Zecchina, G. Spoto, S. Coluccia, E. Garrone, J. Chem. Phys. 80 (1984) 467.
[36] L. Poul, Thèse de doctorat, Université Pierre et Marie Curie (2000).
[37] K. Klier, Langmuir 4 (1988) 13.
[38] B.M. Weckhuysen, R.A. Schoonheydt, in: B.M. Weckhuysen, P. Van der Voort, G. Catana (Eds.), Spectroscopy of Transition Metal Ions on Surfaces, Leuwen Univ. Press, 2000, p. 221.
[39] A. Verbeckmoes, B.M. Weckhuysen, R.A. Schoonheydt, Micropor. Mesopor. Mater. 22 (1998) 165.
[40] E.J. Baran, A.G. Nord, E. Diemann, T. Ericsson, Acta Chem. Scand. 44 (1990) 513;
E.J. Baran, A.G. Nord, E. Diemann, J. Phys. Chem. Solids 50 (1989) 983.
[41] R. Pappalardo, D.L. Wood, R.C. Linares, J. Chem. Phys. 35 (1961) 2041.
[42] I.J. Ardelean, G. Llonca, V. Simon, S. Filip, S. Simon, J. Alloys Compd. 326 (2001) 121.
[43] J. Matsuda, K. Kojima, H. Yano, H. Marusawa, J. Non-Cryst. Solids 111 (1989) 63.
[44] R.A. Verhelst, R.W. Kline, A.M. Graaf, H.O. Hooper, Phys. Rev. B 11 (1975) 4427.
[45] P. Cossee, A.E. Van Arkel, J. Phys. Chem. Solids 15 (1960) 1.
[46] T.J. Chuang, C.R. Brundle, D.W. Rice, Surf. Sci. 59 (1976) 413.
[47] NIST Standard Reference Database 20, Version 3.4 (Web Version). Data compiled and evaluated by C.D. Wagner, A.V. Naumkin, A. Kraut-Vass, J.W. Allison, C.J. Powell, J.R. Rumble Jr.
[48] P. Concepción, A. Galli, J.M. López Nieto, A. Dejoz, M.I. Vasquez, Top. Catal. 3 (1996) 451.
[49] T. Blasco, J.M. Lopez Nieto, Appl. Catal. A 157 (1997) 117;
M.A. Banarès, Catal. Today 51 (1999) 319.
[50] M. Che, M. Tench, Adv. Catal. 32 (1983) 1;
Z. Sojka, E. Giamello, M. Che, A. Zecchina, K. Dyrek, J. Phys. Chem. 92 (1988) 1541.
[51] T. Takahashi, S. Tanase, O. Yamamoto, Electrochim. Acta 23 (1978) 369.
[52] A. Bouhaouss, A. Laghzizil, A. Bensouad, M. Ferhat, G. Lorent, J. Livage, Int. J. Inorg. Mater. 3 (2001) 743.
[53] M. Rouimi, M. Ziyad, J. Leglise, Phosphorus Res. Bull. 10 (1999) 418.